Observation of subnanometre-high surface topography with X-ray reflection phase-contrast microscopy

PAUL FENTER[1]*, CHANGYONG PARK[1], ZHAN ZHANG[1] AND STEVE WANG[2]

[1]Argonne National Laboratory, CHM-200, 9700 South Cass Avenue, Argonne, Illinois 60439, USA

[2]Xradia, Inc., 5052 Commercial Circle, Concord, California 94520, USA

*e-mail: fenter@anl.gov

Published online: 24 September 2006; doi:10.1038/nphys419

The direct observation of molecular-scale features has been the exclusive realm of electron and probe microscopies[1–3], whereas X-ray imaging has been limited to the observation of objects greater than 10 nm in size[4–9] associated with the resolution of X-ray optics. Here, we describe a novel approach that extends hard X-ray microscopy to image the distribution of molecular-scale interfacial features directly and non-invasively with full-field imaging. Interfacial phase contrast from elementary defect structures allows direct observation of 0.6-nm-high monomolecular steps at a solid surface. This non-invasive technique opens up new opportunities to study interfacial processes *in situ* and in real time, particularly those taking place under aggressive chemical conditions, which currently can only be studied by *ex situ* approaches.

Interfacial reactivity is central to many natural and industrial processes. For example, reactions at mineral surfaces control the release of primary nutrients, transport of contaminants in natural waters and the formation of bone and skeletal minerals[10,11]; corrosion constitutes a major industrial cost, including the transportation and production of petroleum products, operation of power plants and the stability of nuclear materials[12,13]; and heterogeneous catalysis may mitigate the effects of fossil-fuel consumption through the development of catalysts with high efficiency and selectivity due to nanoparticle size and shape[14,15].

A necessary requirement for understanding interfacial reactivity is the ability to distinguish elementary steps from terraces, but these phenomena take place in complex environments that are inaccessible to most high-spatial-resolution interfacial probes. Scanning probe microscopy is widely used to image interfacial reactivity in non-vacuum environments[1,16] but its application is often limited by the need for a probe tip (for example, tip-induced artefacts, tip reactivity or the inability to reach buried solid–solid interfaces). Optical interferometry can observe topographical changes to interfaces in contact with fluids but without sensitivity to individual molecular-scale features[17]. Electron microscopy is largely limited to vacuum environments[2,3,18,19]. X-rays and neutrons offer substantial opportunities as non-invasive probes in complex environments due to their highly penetrating nature and direct sensitivity to molecular-scale features, but have relied mostly on spatially averaging measurements such as X-ray scattering and spectroscopy[20–22].

The recent development of X-ray sources and optics has led to new opportunities to image structures and processes using X-ray microscopy[4,8,9,23]. Application of these approaches has been limited, however, to observation of meso- and nanoscopic structures (for example, as small as tens of nanometres)[5–7,24–27] due to limitations in the resolution of X-ray optics. Here, we report a novel approach using X-ray phase contrast derived from elementary defects as a distinct method for imaging the spatial distribution of molecular-scale interfacial features with full-field X-ray microscopy, similar to interfacial electron microscopies[2,19]. We illustrate this approach by imaging elementary steps on a surface using a specularly reflected X-ray beam, with the experimental geometry shown schematically in Fig. 1. This X-ray reflection interface microscope (XRIM) focuses a monochromatic X-ray undulator beam using a condenser Fresnel zone plate (FZP) lens[4] to a small, approximately micrometre-sized, spot on the sample. A magnified image of the surface is projected on an X-ray area detector with an objective FZP using the weak specularly reflected X-ray beam, thereby imaging the spatial variation of the local X-ray reflectivity across the mineral surface. Sensitivity to vertical changes in surface topography derives from phase contrast, that is, due to the difference in X-ray path length for X-rays reflected from neighbouring terraces on either side of a step (Fig. 1b). Variations in surface topography are therefore seen by the X-ray beam as a pure phase object with a sudden phase change across the step. Kinematic X-ray scattering calculations show the essential strengths and challenges of this approach (Fig. 1c). Whereas hard X-ray imaging normally uses strong transmitted[7] or Bragg-reflected[6] X-ray beams, here, interfacial phase contrast is obtained by imaging the weak interface-reflected X-ray beam that is more than five orders of magnitude weaker than the incident beam. The potentially strong variation in the local reflected intensity due to reflection at a step, with theoretical contrast as high as 100% (Fig. 1c), can effectively

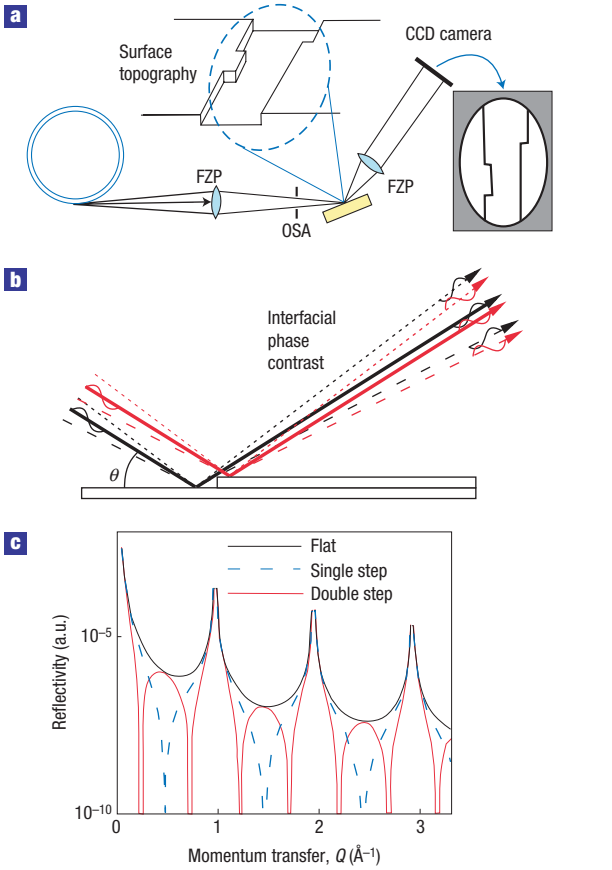

Figure 1 Schematic diagram of the XRIM and mechanism for interfacial phase-contrast imaging a, XRIM instrument with X-ray source, FZP optics, order-sorting aperture (OSA) and charge-coupled device (CCD) camera. The surface topography is shown, inset, and the corresponding reflection image results in dark lines (low reflectivity) in the vicinity of a step. **b**, Schematic diagram of the mechanism for interfacial phase contrast, with a focused X-ray beam reflecting from either side of a step (but within a single resolution volume), resulting in the destructive interference in the far field. **c**, Specular-reflectivity calculations for an ideally smooth surface (black line), and the changes in local reflectivity at monomolecular (dashed blue line) and double-height steps (red line).

compensate for the weak surface reflectivity. Nevertheless, the ability to use phase contrast to image an interface depends critically on the source brilliance and the efficiency of the X-ray optics and detector systems. In spite of these potential difficulties, order of magnitude estimates reveal that images might be obtained in seconds when the reflectivity is $\sim 10^{-5}$, and proportionally longer at lower reflectivity (see Supplementary Information for a detailed description of the system and intensity throughput calculations).

The feasibility of this approach is demonstrated by imaging the (001) surface of orthoclase, $KAlSi_3O_8$, in air at incident angles of $\theta = 1.4°, 1.8°, 2.7°$ and $3.3°$ with a photon energy of 10.0 keV (Fig. 2). Previous studies have shown this surface to be extremely flat with a topography having molecularly sharp steps that are ideal to evaluate the performance of the microscope[28]. The same patterns are observed in each image, including straight lines and an intricate pattern of curved lines. These features seem to arise from the orthoclase surface because the images are obtained by bright-field imaging using the interface-sensitive X-ray reflectivity beam, and wedge-shaped mesa topographies are observed (black arrow, Fig. 2) similar to that seen previously by atomic force microscopy[28]. Sensitivity to bulk defects within the penetration depth of the incident beam (for example, dislocations buried beneath the surface) may also be possible. The observed patterns, however, are identical after correction for angle-dependent perspective as would be expected for two-dimensional structures at different grazing angles (for example, $\sim 1/\sin(\theta)$). This perspective controlled by the grazing angle results in an asymmetry in the spatial resolution within the surface plane (that is, along the vertical and horizontal axes of the images). These images were obtained in ~2–10 min each, and smaller areas were imaged in 10 s with some cost of the signal-to-noise ratio. We expect that similar-quality images can be obtained in <1 s with planned instrumental improvements. Consequently, this provides a way to observe real-time changes to surface topography associated with molecular-scale processes (for example, adsorption, dissolution and precipitation).

An important feature of this approach is that image intensities can be quantified with kinematic diffraction theory. In the present case, the sensitivity to vertical topographical changes (for example, steps) can be derived by considering the phase contrast of X-rays reflected near a step (Fig. 1b). X-rays reflected from neighbouring terraces separated by a monomolecular step are in-phase (that is, invisible) when the momentum transfer, $Q = (4\pi/\lambda)\sin(\theta) = (2\pi/d)L$, corresponds to the Bragg condition, that is, with $L = 1, 2, \ldots$, but are out-of-phase (that is, visible) near the 'anti-Bragg' conditions, $L = 1/2, 3/2$ and so on (where λ is the X-ray wavelength and $d = 0.6464$ nm is the substrate vertical-layer spacing). More generally, the phase change at the step, with height Nd, is characterized by $\Phi = QNd = 2\pi NL$, and the resulting fractional variation of intensity across an N-layer high step (that is, the contrast, C) can be calculated assuming ideal geometrical optics as $C = C_0 \sin^2(\pi NL)$, where C_0 is the maximum contrast (ideally, $C_0 = 1$), allowing step heights to be identified directly. This is illustrated with the isolated curved feature highlighted in Fig. 2, which is chosen because it is largely aligned with the beam direction and the foreshortening of the image due to the perspective view does not complicate the interpretation of resolution. Line scans across the step (Fig. 3a) show that the fractional change in reflectivity varies systematically with the scattering condition (Fig. 3c). The observed contrast variation is well described with $N = 1$, corresponding to a monomolecular step, with a maximum contrast of $C_0 = 0.25$, and is distinct from that for other step heights (for example, a double step, $N = 2$) that show a more rapid oscillation in contrast. This identification is supported by previous studies of the orthoclase–water interface in which wedge-shaped mesas defined by monomolecular steps (black arrow, Fig. 2) are a common feature of cleaved (001) surfaces[28]. Consequently, although the lateral resolution of the microscope is limited by instrumental details (at ~200 nm), the variation of phase contrast with vertical momentum transfer allows this 0.6-nm-high monomolecular step to be identified by intensity contrast. The observed step width at $L = 0.5$ is ~200 nm (indicated by arrows in Fig. 3a), which is twice the expected resolution of the instrument (thereby explaining much, but not all, of the reduced contrast). The reflectivity far from a step, meanwhile, varies strongly with the incident angle and follows the functional form for specular reflectivity determined by the intrinsic molecular-scale interfacial structure[20–22] (Fig. 3d).

We have so far implicitly described the imaging mechanism from an interfacial-scattering perspective, where X-rays scattered by a step will contribute to diffuse scattering[29] at the expense of the specularly reflected X-ray beam. This is complementary to the perspective of geometrical optics, in which the finite numerical aperture of the objective lens will effectively reject any diffuse scattering, thereby leading to a reduction of the local specular

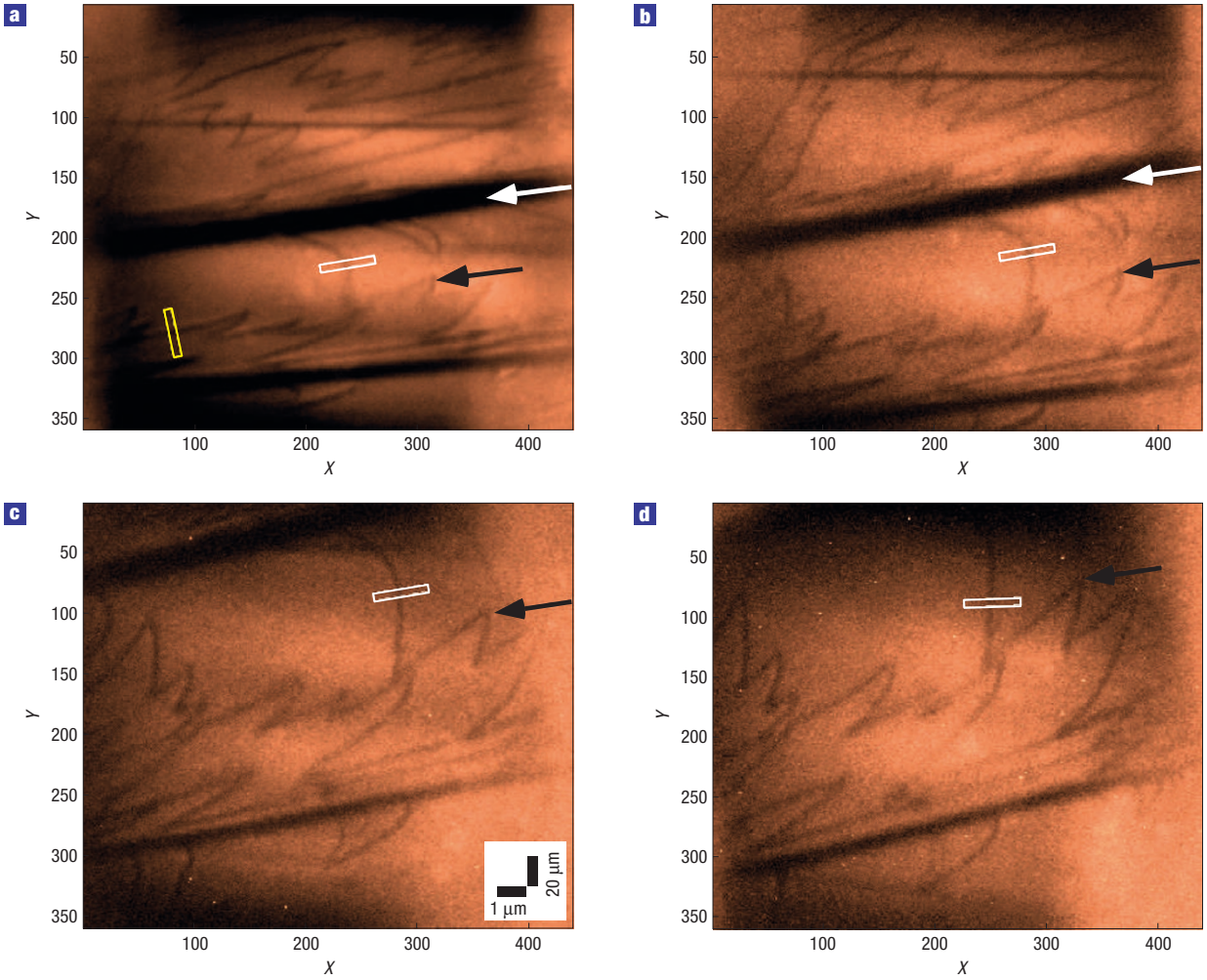

Figure 2 Images of surface topography on an orthoclase (001) surface. a–d, Step distributions imaged at incident angles of 1.4° (**a**), 1.8° (**b**), 2.7° (**c**) and 3.3° (**d**) corresponding to $L = 0.25$, 0.33, 0.49 and 0.60, respectively, using a photon energy of 10 keV, with the scattering plane intersecting the image along the vertical axis. The white and yellow rectangles show areas used to plot line scans in Fig. 3. The black arrow indicates the same wedge-shaped terrace region in each figure, similar to that seen in previous atomic force microscopy studies[28], as well as long straight macro-steps (white arrow). Vertical and horizontal scale bars are indicated in **c**; the horizontal scale for **a**,**b**,**d** is the same as in **c**, but the vertical scale varies with incident angle, θ, due to changes in perspective.

reflectivity near steps with an image contrast that is directly related to the phase change at each step. Evidence that this simple perspective is incomplete is suggested by the intensity variation at steps oriented transverse to the scattering plane (see the line scan in Fig. 3b for the region indicated by the yellow rectangle in Fig. 2a), for instance, in the observation that the local reflectivity near such steps can exceed that of the flat surface far from the step. This effect cannot be easily understood within the context of either interfacial-scattering theory or geometrical optics (because interference due to surface topography is purely destructive within the perspective of kinematic scattering) and is associated with a defocus of the condenser lens of ~5 mm for the images in Fig. 2. As the surface topography is seen by the X-ray beam as a pure phase object, we expect that a truly quantitative understanding of the intensity variation near steps and other defects might be obtained using a more complete simulation of the imaging system in which all experimental details (for example, beam properties, any defocus of the optics and the surface topography) can be properly incorporated.

The present results demonstrate a novel approach for extending X-ray microscopy to observe the distribution of molecular-scale features on a solid surface, in this case elementary steps that are ~300-fold smaller than the experimental resolution. The ability to image elementary steps in real time is expected to lead to new opportunities for understanding interfacial reactivity. For example, observation of step dynamics (for example, during crystal growth and dissolution in aqueous solutions at extreme pH) may provide new information about mineral surface reactivity. Interfacial phase contrast can conceivably be optimized to highlight various structures, including defect distributions at buried solid–solid interfaces (for example, dislocations) and the nucleation and growth of nanoparticles. For instance, nanoparticle Bragg diffraction might identify the growth and habit of particle nucleation (for example, nucleation at steps or on terraces) as might be seen by scanning probe microscopy, but may also be used to identify the crystal phase and orientation of that particle, as would be necessary to understand hetero-epitaxy of particle nucleation and the size-dependent relative stability of

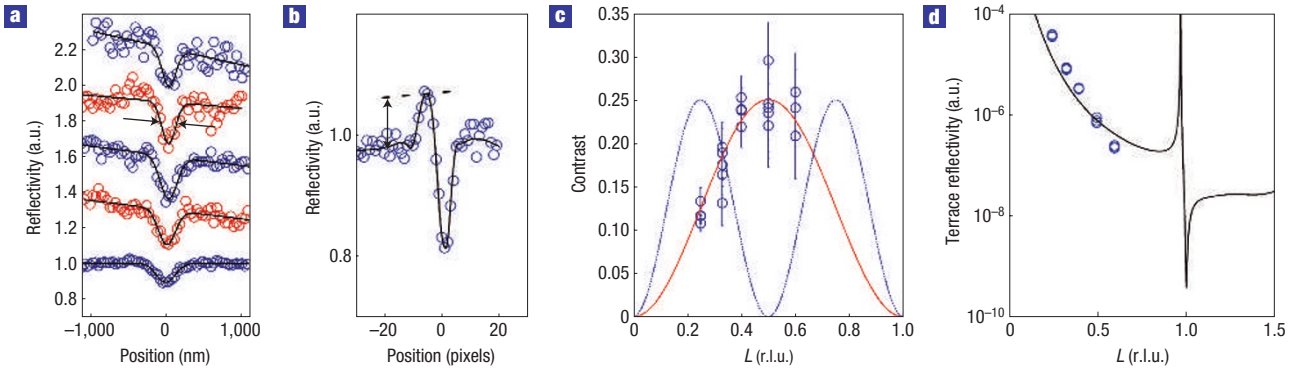

Figure 3 Identification of monomolecular steps by phase contrast. a,**b**, Line scans across features identified by the white (**a**) and yellow (**b**) rectangles in Fig. 2 for incident angles indicated in Fig. 2, and at 2.2° corresponding to $L = 0.4$ (image not shown). The data points show signals (in nominal X-ray counts) that are averaged within the rectangle transverse to the scan direction and normalized to the reflectivity far from a step. The lateral instrumental resolution transverse to the scattering plane is indicated by the arrows in **a**, and the solid lines in **a** are fits with the sum of gaussian and linear functions. The line in **b** is a guide to the eye. **c**,**d**, Observed contrast (**c**) and terrace reflectivity (**d**) as a function of the vertical momentum transfer, L, with multiple data points representing distinct areas along the same step. The lines in **c** are the expected contrast variation for a monomolecular ($N = 1$, solid red line) and double height ($N = 2$, dotted blue line) steps, calculated with $C_0 = 0.25$, and the vertical error bars are the statistical uncertainty in the contrast derived through propagation of errors derived from counting statistics in the CCD images. The line in **d** is the calculated reflectivity (in absolute units) derived from the orthoclase (001) water interface[28] but without fluid water above the surface to approximate the conditions of the experiment. The measured reflectivity data are estimated based on the measured signal and counting time, without corrections for variations in illumination or detector efficiency with an overall scale factor, showing the expected 100-fold variation of signal with vertical momentum transfer.

compositionally equivalent phases (for example, calcite versus aragonite; rutile versus anatase). In a similar way, contrast derived from resonant anomalous dispersion of X-rays may be used to highlight elemental, chemical or magnetic features of an interface that would be useful to probe various interfacial processes such as ion adsorption, corrosion, catalytic reactions, magnetic domain growth and ferroelectric domain switching. In particular, this non-invasive microscope opens up the possibility of observing interfacial reactions under aggressive chemical conditions inaccessible to probe microscopies[30] due to probe-tip reactivity. The ability to measure reflectivity over microscopic regions of a surface also suggests the possibility of carrying out interfacial structural analyses of small-grained materials (for example, clays and zeolites) whose reactivity is important by virtue of their large intrinsic surface area, but whose interfaces have remained largely inaccessible to traditional structural probes. Direct observations of many important interfacial processes may be obtained with this approach, thereby bringing new clarity to many processes that previously could only be understood indirectly through *ex situ*, destructive or spatially averaging measurements.

METHODS

The experiments were carried out at beamline 12-ID-D (BESSRC) at the advanced photon source (APS) at Argonne National Laboratory in December, 2005. The APS undulator was set with its first harmonic at 10 keV. The X-ray beam was reflected from a nominally unfocused horizontal-deflection high-heat-load mirror, and a monochromatic beam with a photon energy of 10.0 keV was selected with a silicon (111) double-bounce monochromator. A detailed description of the microscope design is provided in Supplementary Information. The sample was prepared by cleaving gem-quality orthoclase ($KAlSi_3O_8$) to reveal a fresh (001) surface and mounted on a sample holder and held in place with epoxy. The sample was mounted on a four-circle diffractometer so that the incident angle of the beam with respect to the sample surface could be precisely controlled and measurements were carried out with the sample in contact with air. The reflected beam was imaged using an area detector mounted on the diffractometer detector arm.

Received 5 April 2006; accepted 29 August 2006; published 24 September 2006.

References

1. Ohnesorge, F. & Binnig, G. True atomic-resolution by atomic force microscopy through repulsive and attractive forces. *Science* **260,** 1451–1456 (1993).
2. Bauer, E. Low-energy-electron microscopy. *Rep. Prog. Phys.* **57,** 895–938 (1994).
3. Williams, D. B. & Carter, C. B. *Transmission Electron Microscopy: A Textbook for Materials Science* (Plenum, New York, 1996).
4. Yun, W. *et al.* Development of zone plates with a blazed profile for hard X-ray applications. *Rev. Sci. Instrum.* **70,** 3537–3541 (1999).
5. Larson, B. C., Yang, W., Ice, G. E., Budai, J. D. & Tischler, J. Z. Three-dimensional X-ray structural microscopy with submicrometre resolution. *Nature* **415,** 887–890 (2002).
6. Do, D. H. *et al.* Structural visualization of polarization fatigue in epitaxial ferroelectric oxide devices. *Nature Mater.* **3,** 365–369 (2004).
7. Eisebitt, S. *et al.* Lensless imaging of magnetic nanostructures by X-ray spectro-holography. *Nature* **432,** 885–888 (2004).
8. Chao, W. L., Harteneck, B. D., Liddle, J. A., Anderson, E. H. & Attwood, D. T. Soft X-ray microscopy at a spatial resolution better than 15 nm. *Nature* **435,** 1210–1213 (2005).
9. Kang, H. C. *et al.* Nanometer linear focusing of hard X-rays by a multilayer Laue lens. *Phys. Rev. Lett.* **96,** 127401 (2006).
10. Stumm, W., Sigg, L. & Sulzberger, B. *Chemistry of the Solid-Water Interface: Processes at the Mineral-Water and Particle-Water Interface in Natural Systems* (Wiley, New York, 1992).
11. Brown, G. E. & Parks, G. A. Sorption of trace elements on mineral surfaces: Modern perspectives from spectroscopic studies, and comments on sorption in the marine environment. *Int. Geol. Rev.* **43,** 963–1073 (2001).
12. Marcus, P. Surface science approach of corrosion phenomena. *Electrochim. Acta* **43,** 109–118 (1998).
13. Long, J. C. S. & Ewing, R. C. Yucca mountain: Earth-science issues at a geologic repository for high-level nuclear waste. *Annu. Rev. Earth Planet. Sci.* **32,** 363–401 (2004).
14. Valden, M., Lai, X. & Goodman, D. W. Onset of catalytic activity of gold clusters on titania with the appearance of nonmetallic properties. *Science* **281,** 1647–1650 (1998).
15. Xu, Z. *et al.* Size-dependent catalytic activity of supported metal-clusters. *Nature* **372,** 346–348 (1994).
16. Gratz, A. J., Manne, S. & Hansma, P. K. Atomic force microscopy of atomic-scale ledges and etch pits formed during dissolution of quartz. *Science* **251,** 1343–1346 (1991).
17. Luttge, A., Bolton, E. W. & Lasaga, A. C. An interferometric study of the dissolution kinetics of anorthite: The role of reactive surface area. *Am. J. Sci.* **299,** 652–678 (1999).
18. Leslie, C. *et al.* Electron crystallography in surface structure analysis. *Microsc. Res. Techniq.* **46,** 160–177 (1999).
19. Buseck, P., Cowley, J. M. & Eyring, L. *High-Resolution Transmission Electron Microscopy and Associated Techniques* (Oxford Univ. Press, New York, 1988).
20. Als-Nielsen, J. & McMorrow, D. *Elements of Modern X-ray Physics* (Wiley, Chichester, 2001).
21. Robinson, I. K. & Tweet, D. J. Surface X-ray-diffraction. *Rep. Prog. Phys.* **55,** 599–651 (1992).
22. Fenter, P. A. X-ray reflectivity as a probe of mineral-fluid interfaces: A user guide. *Rev. Mineral. Geochem.* **49,** 149–220 (2002).
23. Jacobsen, C. & Kirz, J. X-ray microscopy with synchrotron radiation. *Nature Struct. Biol.* **5,** 650–653 (1998).
24. Myneni, S. C. B., Brown, J. T., Martinez, G. A. & Meyer-Ilse, W. Imaging of humic substance macromolecular structures in water and soils. *Science* **286,** 1335–1337 (1999).
25. Benzerara, K., Yoon, T. H., Menguy, N., Tyliszczak, T. & Brown, G. E. Nanoscale environments associated with bioweathering of a Mg-Fe-pyroxene. *Proc. Natl Acad. Sci. USA* **102,** 979–982 (2005).
26. Bilderback, D. H., Hoffman, S. A. & Thiel, D. J. Nanometer spatial-resolution achieved in hard X-ray-imaging and Laue diffraction experiments. *Science* **263,** 201–203 (1994).

27. Tamura, N. *et al.* High spatial resolution grain orientation and strain mapping in thin films using polychromatic submicron x-ray diffraction. *Appl. Phys. Lett.* **80,** 3724–3726 (2002).
28. Teng, H. H., Fenter, P., Cheng, L. W. & Sturchio, N. C. Resolving orthoclase dissolution processes with atomic force microscopy and X-ray reflectivity. *Geochim. Cosmochim. Acta* **65,** 3459–3474 (2001).
29. Sinha, S. K., Sirota, E. B., Garoff, S. & Stanley, H. B. X-Ray and neutron-scattering from rough surfaces. *Phys. Rev. B* **38,** 2297–2311 (1988).
30. Jordan, G. *et al.* Acidic dissolution of plagioclase: *In situ* observations by hydrothermal atomic force microscopy. *Geochim. Cosmochim. Acta* **63,** 3183–3191 (1999).

Acknowledgements

This work was supported by the Department of Energy, Office of Basic Energy Sciences, Division of Chemical Sciences, Geosciences and Biosciences, Geosciences Research Program through contract W-31-109-ENG-38 to Argonne National Laboratory. Measurements were done at beamline 12-ID-D (BESSRC) at the Advanced Photon Source, which is supported by the Department of Energy, Office of Basic Energy Sciences. We thank W. Yun and M. Feser (Xradia) for their assistance in the design and construction of the X-ray optics, N. C. Sturchio for a careful reading of the manuscript, J. Catalano for assistance during the measurement, the BESSRC group for assistance and Jeremy Levy for providing test samples.
Correspondence and requests for materials should be addressed to P.F.
Supplementary Information accompanies this paper on www.nature.com/naturephysics.

Competing financial interests

The authors declare that they have no competing financial interests.